JOURNAL OF SPACECRAFT AND ROCKETS
Vol. 31, No. 1, January–February 1994

Drag Reduction for Turbulent Flow over a Projectile: Part I

Jan-Kaung Fu*
Chinese Air Force Academy, Kangshan, Kaohsiung, Taiwan 82012, Republic of China
and
Shen-Min Liang†
National Cheng Kung University, Tainan, Taiwan, Republic of China

A numerical study is made to analyze the drag performance of a secant-ogive-cylinder-boattail projectile in the transonic Mach number regime between 0.91 and 1.20. To improve the projectile's performance, two drag reduction methods, boattailing and base bleed, are applied. The effectiveness of each method and the combination of both methods are studied by varying the values of parameters such as boattail angle, bleed quantity, and bleed area. The computed distributions of surface pressure coefficient of the projectile with different boattail angles are in close agreement with experimental data. Computed drag components and the total drag of the projectile are accurate by comparison with experimental data and semiempirical predictions. The optimal boattail angle for total drag reduction is predicted to be at about 5–7 deg. The method of combining boattailing and base bleed can become an effective method for total drag reduction.

Nomenclature

a = speed of sound
a_ξ^m = eigenvalues of Jacobian matrix $\hat{A}$
C_f = skin friction coefficient
C_{D0} = total drag coefficient
C_{DB} = base drag coefficient
C_{DBT} = boattail drag coefficient
C_{DH} = head (or nose) drag coefficient
C_{DP} = pressure drag coefficient, $C_{DH} + C_{DBT}$
C_{DV} = viscous (or skin friction) drag coefficient
C_p = pressure coefficient, $2(p - p_\infty)/(\rho_\infty u_\infty^2)$
CFL = Courant number
D = numerical dissipation function or diameter of projectile
$\hat{E}, \hat{F}, \hat{G}$ = components of flux vector in curvilinear coordinates
$\tilde{E}, \tilde{G}$ = numerical flux function
e = total energy per unit volume
$\hat{H}$ = source term reduced from $\partial\hat{F}/\partial\eta$
h = time step, Δt
I = identity matrix or bleed rate in base bleed
J = Jacobian defined as $J^{-1} = R(x_\zeta R_\zeta - x_\zeta R_\xi)$
M = Mach number or grid number in streamwise direction
N = $T_\xi^{-1} T_\zeta$
Pr = Prandtl number
p = static pressure
$\hat{Q}$ = column vector of conservative variables in curvilinear coordinates
R = radial coordinate
Re = Reynolds number, $\rho_\infty u_\infty D/\mu_\infty$
$\hat{S}$ = viscous flux vector in ζ direction
T_ξ = matrix whose column consists of eigenvectors of $\hat{A}$
T_ζ = matrix whose column consists of eigenvectors of $\hat{C}$
t = time
U, V, W = contravariant velocity components in curvilinear coordinates
u, v, w = Cartesian velocity components in Cartesian coordinates
x, y, z = Cartesian coordinates
β = boattail angle
γ = ratio of specific heats
ξ, η, ζ = curvilinear coordinates
Λ = diagonal matrix of eigenvalues
$\lambda^\xi, \lambda^\zeta$ = $\Delta t/\Delta\xi$, $\Delta t/\Delta\zeta$
μ = dynamic viscosity
ρ = density
ϕ = angle in η direction
Ω = spin rate

Subscripts

n = normal component to surface
∞ = freestream condition

Superscripts

$*$ = temporary state
m = mth element of a vector or a diagonal matrix
n = nth time step
$()^{-1}$ = inverse of the argument inside parenthesis

Received June 17, 1991; revision received Sept. 13, 1991; accepted for publication Sept. 24, 1991.

*Associate Professor, Department of Aeronautics.
†Associate Professor, Institute of Aeronautics and Astronautics. Member AIAA.

Introduction

AXISYMMETRIC bodies like missiles, artillery projectiles, and bullets often have a blunt base. The corresponding base drag is usually an appreciable part of the total drag. The capability to determine the aerodynamics of a projectile is required over a wide flight range. The critical aerodynamic behavior of projectiles in the transonic regime can be attributed in part to the formation of shock waves. The range and terminal velocity of a projectile are two critical factors in shell design that are directly related to the total aerodynamic drag. The total drag for projectiles can be divided into three components: 1) pressure (or wave) drag (excluding the base region), 2) viscous (or skin friction) drag, and 3) base drag. For a typical shell at $M_\infty = 0.9$, the relative magnitude of the aerodynamic drag components are 20% pressure drag, 30% viscous drag, and 50% base drag.[1,2] Thus, the determination of base drag is essential in predicting the total drag for projectiles.

The pressure and viscous components of drag generally cannot be reduced significantly without adversely affecting the stability of the shell; consequently, efforts to reduce the total drag have been directed toward reducing the base drag. A significant amount of work in this direction has been done in the past three decades. A number of studies have been made that show, for axisymmetric base flow, the only methods for reducing base drag seem to be boattailing and base bleed or mass injection.[3,4] Although in the transonic regime an additional wave drag is induced by the shock wave developed on the boattail portion, nevertheless boattailing can effectively reduce the base drag by reducing the area of the base and the extent of flow expansion at the base corner.[3-5] The second feasible method in the base drag reduction is base bleed, in which a small amount of mass flow is injected into the base region to increase the base pressure. This concept of mass injection at the projectile base has been widely studied for supersonic flows,[6-10] whereas fewer data are available in the transonic flow regime.[1,5]

In the past 15 years, a theoretical and experimental research program has been underway to provide the capability for predicting projectile aerodynamics. Earlier efforts were predominantly in the supersonic regime, but in recent years[11,12] efforts have been extended to the transonic regime. In experiments, the individual drag components, especially the base drag and skin friction drag, are difficult to measure. Two design codes, MCDRAG[13] and NSWCAP,[14,15] based on semiempirical techniques, are available for quickly predicting individual drag component and the total aerodynamic drag; however, the design codes appear inaccurate in the transonic regime because of limited experimental data. On the other hand, due to the rising cost of experimental measurements (together with limited transonic facilities) and the recent advances in computer processors, significant progress in numerical procedures[1,16-18] has been made. Hence, numerical simulation is a "good" approach for predicting all individual drag components for projectiles on a cost-effective basis.

Traditional schemes, such as central differencing schemes, can produce numerical oscillations near shock waves and need special tuning of the artificial viscosity for damping out the numerical oscillations. To avoid the numerical oscillations near the shock, an implicit diagonalized symmetric total variation diminishing (TVD) scheme[19,20] is employed to solve the thin-layer axisymmetric Navier-Stokes equations associated with the Baldwin-Lomax turbulence model.[21]

A sequence of studies has been made to reduce the total drag for transonic projectiles by various methods. In Part I, the numerical solver associated with boattailing and base bleed is described. The overall flow structure of turbulent transonic projectiles obtained by this flow solver is explored. The accuracy of the predicted drag components is assessed. Finally, the parameters used in boattailing and base bleed are optimized. In Part II, a drag reduction method of combining boattailing and passive control of shock/boundary-layer interaction will be reported.

Mathematical Formulation—Axisymmetric Thin-Layer Navier-Stokes Equations

For an axisymmetric projectile at zero angle of attack, the equations governing the flow are the azimuthal-invariant Navier-Stokes equations, which can be obtained from the three-dimensional Navier-Stokes equations. Figure 1 shows the notation for the Cartesian coordinates x, y, z, the cylindrical coordinates x, ϕ, R, and the transformed coordinates ξ, η, ζ, where ξ, η, and ζ represent the longitudinal, the circumferential, and the near-normal coordinates, respectively. The transformed axisymmetric thin-layer Navier-Stokes equations can be written as[22]

$$\partial_t \hat{Q} + \partial_\xi \hat{E} + \partial_\zeta \hat{G} + \hat{H} = Re^{-1}\partial_\zeta \hat{S} \tag{1}$$

where

$$\hat{Q} = J^{-1}\begin{bmatrix}\rho\\ \rho u\\ \rho v\\ \rho w\\ e\end{bmatrix}, \qquad \hat{E} = J^{-1}\begin{bmatrix}\rho U\\ \rho uU + \xi_x p\\ \rho vU + \xi_y p\\ \rho wU + \xi_z p\\ U(e+p)\end{bmatrix}$$

$$\hat{G} = J^{-1}\begin{bmatrix}\rho W\\ \rho uW + \zeta_x p\\ \rho vW + \zeta_y p\\ \rho wW + \zeta_z p\\ W(e+p)\end{bmatrix}, \qquad \hat{H} = J^{-1}\begin{bmatrix}0\\ 0\\ \rho V(R_\xi U + R_\zeta W)\\ -\rho V^2 R - p/R\\ 0\end{bmatrix} \tag{2a}$$

$$\hat{S} = J^{-1}\begin{bmatrix}0\\ \mu m_1 u_\zeta + (\mu/3)m_2\zeta_x\\ \mu m_1 v_\zeta + (\mu/3)m_2\zeta_y\\ \mu m_1 w_\zeta + (\mu/3)m_2\zeta_z\\ \mu m_1 m_3 + (\mu/3)m_2(\zeta_x u + \zeta_y v + \zeta_z w)\end{bmatrix}$$

with

$$\begin{aligned} m_1 &= \zeta_x^2 + \zeta_y^2 + \zeta_z^2\\ m_2 &= \zeta_x u_\zeta + \zeta_y v_\zeta + \zeta_z w_\zeta\\ m_3 &= (u^2 + v^2 + w^2)_\zeta/2 + Pr^{-1}(a^2)_\zeta/(\gamma - 1)\end{aligned} \tag{2b}$$

and

$$\begin{aligned} U &= \xi_x u + \xi_y v + \xi_z w\\ V &= \eta_x u + \eta_y v + \eta_z w\\ W &= \zeta_x u + \zeta_y v + \zeta_z w\end{aligned} \tag{2c}$$

Here U, V, and W are the contravariant velocity components, and the Jacobian J is defined as

$$J^{-1} = R(x_\xi R_\zeta - x_\zeta R_\xi) \tag{2d}$$

Let computations be performed on the $\phi = 0$ plane. Then, in Eq. (2d), $R = z$, $R_\xi = z_\xi$, and $R_\zeta = z_\zeta$ for $\phi = 0$. The metric terms ξ_y, η_x, η_z, and ζ_y are zero when Eqs. (2a–2c) are used, and the rest of the metric terms can be found in Ref. 22.

Although Eq. (1) contains only two spatial derivatives, it retains all three momentum equations and allows a degree of generality over the standard axisymmetric equations. In particular, the circumferential velocity is not assumed to be zero, thus computations for spinning projectiles or swirling flow can be accomplished.

It should be noted that for high Reynolds number turbulent flows of projectiles the validity of the thin-layer approximation was verified by Degani and Schiff,[23] but the use of the thin-layer approximation can save more computational time compared with the full Navier-Stokes equations. The two-layer algebraic turbulence model of Baldwin-Lomax[21] for eddy viscosity is employed. The advantage of this turbulence model is that it is simple to implement and there is no need to determine the outer edge of the boundary layer before the model can be applied.

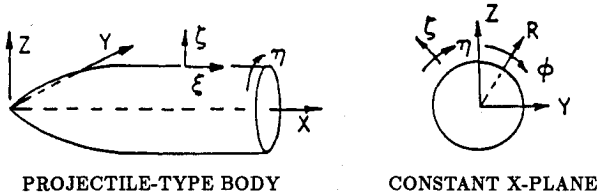

Fig. 1 System of curvilinear coordinates for a projectile.

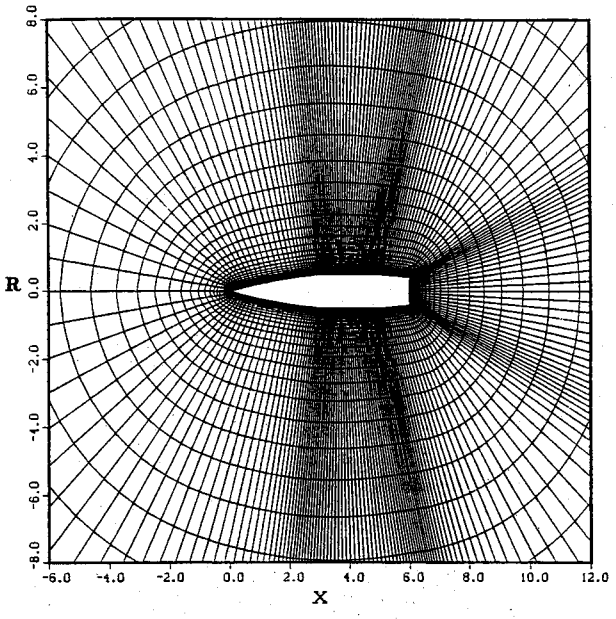

Fig. 2 Grid generated for an SOCBT projectile.

Grid Generation

Interactions between shock waves and the boundary layer make the flow more complicated for projectiles at transonic speeds. Thus, an appropriate numerical grid is important for obtaining the relevant physics of the problem. The boundary-layer development near the wall is critical and the grid should be fine enough to resolve the viscous effects and the shock-wave/boundary-layer interaction. In general, the O-type grid is used for the projectile with a base.[24] In this study, the grid-generation procedure includes the numerical approach of Sorenson's elliptic solver[25] and a simple tangent stretching interpolation method.[26] Once the coordinates of the body and the outer boundary are specified, the elliptic solver is used to generate a grid (in the ζ direction). Then the stretching interpolation is used to obtain a final grid, as shown in Fig. 2, on which grid points are clustered near the body surface and stretched in the far field.

Numerical Procedure

Approximate Factorization

The approximate factorization method of Beam and Warming[27] is applied to Eq. (1) to obtain a semi-finite-difference equation

$$(I + h\partial_\xi \hat{A}^n)(I + h\partial_\zeta \hat{C}^n - hRe^{-1}\partial_\zeta J^{-1}\hat{M}^n)\Delta\hat{Q}^n$$
$$= -h(\partial_\xi \hat{E}^n + \partial_\zeta \hat{G}^n + \hat{H}^n - Re^{-1}\partial_\zeta \hat{S}^n) = \hat{R}(\hat{Q}^n) \qquad (3)$$

where $\hat{A}$, $\hat{C}$, and $\hat{M}$ are the Jacobian matrices defined as

$$\hat{A} = \frac{\partial \hat{E}}{\partial \hat{Q}}, \quad \hat{C} = \frac{\partial \hat{G}}{\partial \hat{Q}}, \quad \hat{M} = \frac{\partial \hat{S}}{\partial \hat{Q}}$$

Equation (3) contains two implicit operators in which each operator will produce a block-tridiagonal matrix. The inversion of the block-tridiagonal matrices is the most time-consuming part of the computation. The overall computational work of this part can be decreased by introducing a diagonalization of the blocks in the implicit operators as developed by Pulliam and Chaussee[28] and by neglecting the viscous flux Jacobian.[29,30] Since $\hat{A}$ and $\hat{C}$ can be diagonalized, $\hat{A} = T_\xi \Lambda^\xi T_\xi^{-1}$ and $\hat{C} = T_\zeta \Lambda^\zeta T_\zeta^{-1}$, where matrices T_ξ and T_ζ consist of the right eigenvectors of $\hat{A}$ and $\hat{C}$, respectively, and the elements of diagonal matrices Λ^ξ and Λ^ζ are the corresponding eigenvalues. After neglecting the viscous Jacobian on the implicit side and factoring the similarity matrices T_ξ and T_ζ outside the spatial derivatives ∂_ξ and ∂_ζ, one obtains

$$T_\xi(I + h\partial_\xi \Lambda^\xi)T_\xi^{-1} T_\zeta(I + h\partial_\zeta \Lambda^\zeta)T_\zeta^{-1}\Delta\hat{Q}^n = R(\hat{Q}^n) \qquad (4)$$

Symmetric Total Variation Diminishing Method

Let $t = n\Delta t$, $\xi = j\Delta\xi$, $\zeta = l\Delta\zeta$, $\lambda^\xi = \Delta t/\Delta\xi$, $\lambda^\zeta = \Delta t/\Delta\zeta$, and $a^m_{j+\frac{1}{2}}$, $T_{j+\frac{1}{2}}$, and $T^{-1}_{j+\frac{1}{2}}$ denote the quantities a^m_ξ, T_ξ, and T_ξ^{-1} evaluated at $\hat{Q}_{j+\frac{1}{2},l}$. Hence, the values of $\hat{Q}_{j+\frac{1}{2},l}$ and $\hat{Q}_{j,l+\frac{1}{2}}$ are evaluated at the cell surfaces, respectively, using Roe's averaging procedure.[31] The final diagonalized form of the symmetric TVD scheme can be written in the form[19,32]

$$[I + \lambda^\xi(M^\xi_{j+\frac{1}{2},l} - M^\xi_{j-\frac{1}{2},l})]\Delta\hat{Q}^* = T_\xi^{-1}\hat{R}(\hat{Q}^n) \qquad (5a)$$

$$[I + \lambda^\zeta(M^\zeta_{j,l+\frac{1}{2}} - M^\zeta_{j,l-\frac{1}{2}})]\Delta\hat{Q}^{**} = N^{-1}\hat{Q}^* \qquad (5b)$$

$$\hat{Q}^{n+1} = \hat{Q}^n + T_\zeta\Delta\hat{Q}^{**} \qquad (5c)$$

The detailed form of M can be found in Ref. 32.

The term $\hat{R}(\hat{Q}^n)$ on the right-hand side of Eq. (5a) is of the form

$$\hat{R}(\hat{Q}^n) = -\lambda^\xi(\tilde{E}^n_{j+\frac{1}{2},l} - \tilde{E}^n_{j-\frac{1}{2},l}) - \lambda^\zeta(\tilde{G}^n_{j,l+\frac{1}{2}} - \tilde{G}^n_{j,l-\frac{1}{2}})$$
$$- h\hat{H}^n + Re^{-1}\lambda^\zeta(\hat{S}^n_{j,l+\frac{1}{2}} - \hat{S}^n_{j,l-\frac{1}{2}}) \qquad (6)$$

where the numerical flux function $\tilde{E}_{j+\frac{1}{2},l}$ can be expressed as[33]

$$\tilde{E}_{j+\frac{1}{2},l} = \tfrac{1}{2}(\hat{E}_{j+1,l} + \hat{E}_{j,l} + D_{j+\frac{1}{2}}/J_{j+\frac{1}{2}}) \qquad (7)$$

and $D_{j+\frac{1}{2}}$ is the explicit dissipation term. The definition of D can be referred to Ref. 19.

Boundary and Initial Conditions

Impermeable Wall Boundary Condition

The body surface is mapped to the constant ζ line in the computational domain. On the impermeable surface of a rigid body without spin, the no-slip condition must be satisfied. For an axisymmetric body spinning with angular velocity Ω, the no-slip condition is $U = W = 0$ and $V = \Omega$. The Cartesian velocity components u, v and w can be solved from the following relation:

$$\begin{bmatrix} u \\ v \\ w \end{bmatrix} = J^{-1} \begin{bmatrix} \eta_y\zeta_z & 0 & -\eta_y\zeta_z \\ 0 & (\xi_x\zeta_z - \xi_z\zeta_x) & 0 \\ -\eta_y\xi_x & 0 & \eta_y\xi_x \end{bmatrix} \begin{bmatrix} U \\ V \\ W \end{bmatrix} \qquad (8)$$

The surface pressure is determined from the assumption that the normal pressure gradient at the body surface is zero:

$$p_n\sqrt{\zeta_x^2 + \zeta_z^2} = (\xi_x\zeta_x + \xi_z\zeta_z)p_\xi + (\zeta_x^2 + \zeta_z^2)p_\zeta = 0 \qquad (9)$$

where n denotes the normal direction of the body surface. The total energy e is obtained from the following equation:

$$e = \frac{p}{\gamma - 1} + \tfrac{1}{2}\rho(u^2 + v^2 + w^2) \qquad (10)$$

Permeable Wall Boundary Condition

For projectiles with base bleed, the ejected mass flux is specified on the body surface. Because of the absence of a measured wall bleed distribution, a uniform distribution of surface bleed is employed. The amount of air injected into the base region is specified by the mass flow rate $\dot{m}_j$ ($= \rho_j u_j A_j$). Rather than specifying $\dot{m}_j$, however, it is customary and convenient to specify the bleed quantity I that is defined as

$$I = (\rho u)_j \bar{\omega}/M_\infty \qquad (11)$$

where $\bar{\omega}$ is the area ratio A_j/A_b, with A_b the base area and A_j the bleed area. Note that both the bleed quantity I and the area ratio $\bar{\omega}$ are two parameters in the base bleed method for the base drag reduction. Given I, $\bar{\omega}$, and M_∞ and the extrapolated density ρ_j from the first interior point off the body surface, the injection velocity u_j can be calculated from Eq. (11), and v and w are set to zero.

Far-Field Boundary Condition

The far-field boundary condition is imposed at $\zeta = \zeta_{\max}$ for an O-type grid system. On the inflow boundary ($W_{\zeta_{\max}} \leq 0$), all physical variables Q_i are fixed at freestream values for both supersonic and subsonic flows. On the outflow boundary ($W_{\zeta_{\max}} > 0$), all variables Q_i are extrapolated from the first interior point off the outer boundary for $M_\infty > 1$, whereas for $M_\infty < 1$, the same conditions used in supersonic flow are used except that the total energy e is obtained from Eq. (10) with fixed freestream pressure p_∞ and the other extrapolated quantities.

Numerical Boundary Condition

The symmetry condition is applied on the centerline of the body of revolution ahead of the nose ($\xi = 0$) and aft of the base ($\xi = \xi_{\max}$), a second-order extrapolation is used such that $\partial_\xi \rho = \partial_\xi (\rho u) = \partial_\xi (\rho v) = \partial_\xi e = 0$, and the momentum in the z direction (ρw) is set to zero.

Initial Condition

The convergence of steady-state solutions is strongly influenced by the choice of initial conditions. A well-selected initial guess provides less initial error and hence a faster convergence rate. In this study, all flow variables are set to the freestream values initially, then the boundary conditions are enforced gradually during the iteration process. This slow impulsive start accompanied with a smaller value of *CFL* helps to reduce the initial transient errors, especially for viscous flows.

Selection of Time Step

For steady-state calculations, a spatially varying time step is used to obtain a fast converged solution. This is an effective strategy for a grid system with spacing varying from very fine to very coarse. The stability criterion for an explicit scheme is used for the present implicit scheme with larger Courant number *CFL*. The time step varies according to[34]

$$\Delta t = CFL/[|U| + |W| + a\sqrt{\xi_x^2 + \xi_z^2} + a\sqrt{\zeta_x^2 + \zeta_z^2}] \quad (12)$$

where a is the local speed of sound. The value of *CFL* is chosen between 1.5 and 3.0 for fast convergence. At the first 50 iterations, a smaller *CFL* (around 1.0) is used. As the iteration proceeds, the Courant number is increased to a larger value.

Results and Discussion

Transonic turbulent flows past a secant-ogive-cylinder-boattail (SOCBT) projectile at zero angle of attack are considered. The projectile model has a three-caliber secant-ogive nose followed by a two-caliber cylinder and a one-caliber β-degree boattail. All numerical computations were performed on an ALLIANT computer FX80. A series of computations were based on the conditions of a stagnation temperature of 580°R and a Reynolds number of 4.6×10^6 based on the model length. Steady-state solutions are achieved when the residual measured by the root-mean-square error in all five conservative variables is less than 1.5×10^{-5}. The axisymmetric projectile flows are computed on the $\phi = 0$ plane, and the flow domain chosen has an outer boundary about 25 calibers from the projectile. The computational grid used has 110 points in the streamwise direction and 60 points in the direction normal to the projectile surface. This grid system is clustered near the body surface with a minimum spacing of $\Delta\zeta_{\min} = 4.2 \times 10^{-5} D$ to insure that there are at least two grid points inside the laminar sublayer, where D is the diameter of the cylinder. The effectiveness of both boattailing and base bleed methods on drag reduction will be discussed next.

Effect of Boattailing

Five different boattail angles—0, 3, 5, 7, and 8 deg—and six freestream Mach numbers—0.91, 0.94, 0.96, 0.98, 1.1, and 1.2—were chosen in the present study. The selection of boattail angles is to provide a fundamental understanding of the flow characteristics of a projectile in the transonic regime and to see the boattailing effect on the components of the total drag. Only a few cases are presented in this paper. More results can be found in Ref. 35.

Figures 3a and 3b show the Mach number contours of a projectile with 0 and 7 deg boattail angles at a Mach number of 0.96, respectively. For the case of zero boattail angle, the predicted location of the shock wave on the cylinder is found to be in close agreement with the shadowgraph reported by Kayser and Whiton.[11] A strong flow expansion, occurring near the base corner and followed by a shear layer, is well predicted. Because of this fast expansion at the base corner, a

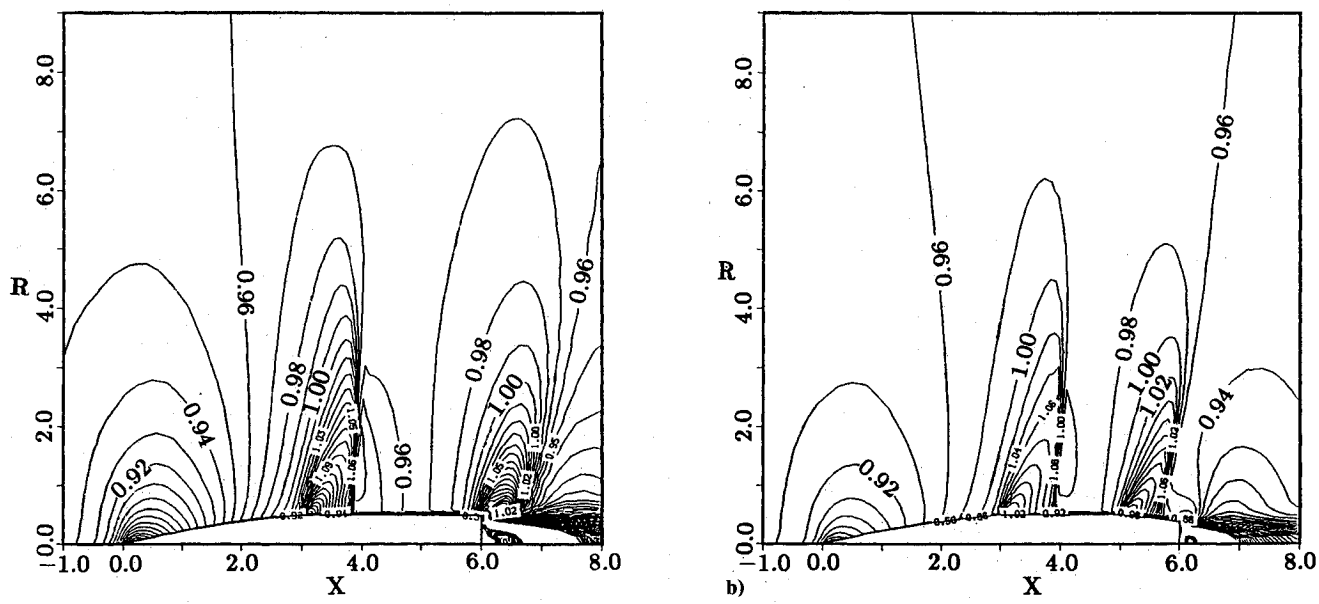

Fig. 3 Mach number contours for turbulent transonic flow over a projectile, $M_\infty = 0.96$: a) $\beta = 0$ deg and b) $\beta = 7$ deg.

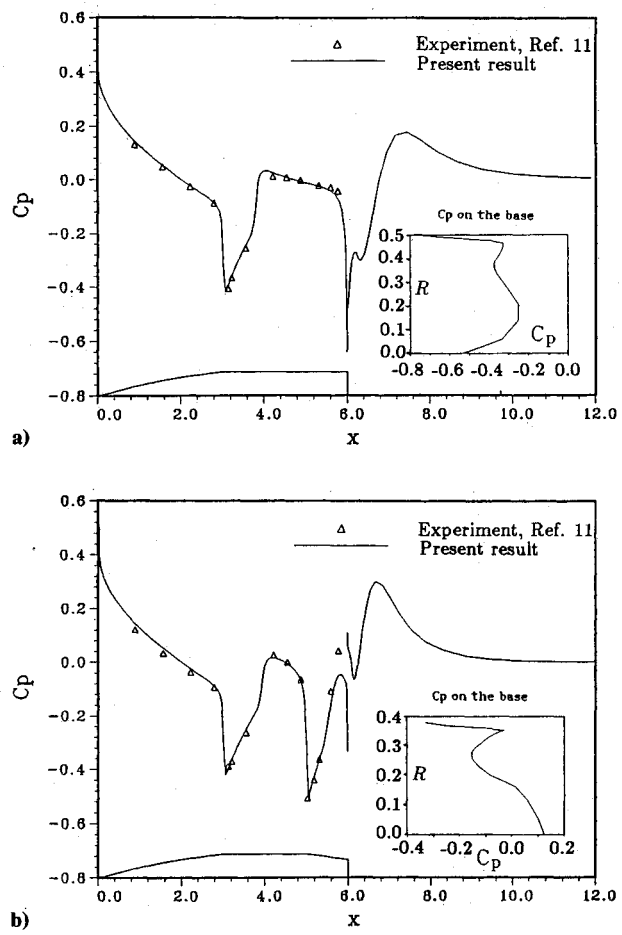

Fig. 4 Distribution of surface pressure coefficient for a projectile, $M_\infty = 0.96$: a) $\beta = 0$ deg and b) $\beta = 7$ deg.

local supersonic region forms near the base corner. This supersonic region for $M_\infty = 0.96$ was found to be larger than the one for the $M_\infty = 0.91$ and 0.94 cases. For the case of supersonic flows, there is no normal shock formed on the cylinder. For the case of 7 deg boattail angle, in addition to the normal shock near the cone-cylinder juncture, a stronger normal shock forms on the boattail. The predicted shock location agreed well with the shadowgraph result of Kayser and Whiton.[11] The extent of flow expansion near the base corner is reduced due to boattailing, resulting in a subsonic region at the base corner. It was found that the recirculatory zone behind the base for the projectile with $\beta = 7$ deg is smaller than that for the projectile with $\beta = 0$ deg. The reattachment length is about $1.3D$ distance from the base (at $x = 6$) for $\beta = 0$ deg and $0.6D$ distance for $\beta = 7$ deg.

The computed distributions of surface pressure coefficient C_p (including the base part) on a projectile for $M_\infty = 0.96$ with $\beta = 0$ and 7 deg are shown in Figs. 4a and 4b, respectively. Good agreement between the predicted and measured pressure coefficients is obtained; slight discrepancies were observed near the projectile base for $\beta = 7$ deg that could be attributed to the interference of the sting used in the measurement. The value of C_p behind the base ($x = 6$) is the pressure coefficient along the symmetry axis, $\xi = \xi_{max}$. The pressure coefficients for $\beta = 0$ and 7 deg along the base are shown in the subplots in Figs. 4a and 4b, respectively. Note that the surface pressure attains a minimum at the base corner where the flow rapidly expands. The pressure along the symmetry axis is increased from the base, reaching a maximum at the reattachment point, and followed by a downstream recovery.

The individual drag component variation with Mach number for projectiles with $\beta = 0$ and 7 deg are obtained from the calculated solutions. Because of space limitation, only the results for the case $\beta = 7$ deg are shown. Figure 5 shows the pressure drag coefficient C_{DP} for $\beta = 7$ deg increases with Mach number (≤ 1.1). The pressure drag, including the pressure drag on the boattail, predicted by the TVD scheme compares well with the experimental results of Kayser[12] and the predictions of the Beam-Warming scheme.[17] But the prediction by the MCDRAG design code[13] is about 10% lower. A larger value of C_{DP} at transonic speeds is predicted by the TVD scheme due to the boattail effect. For $\beta = 0$ deg, the C_{DP} predicted by the present TVD scheme agrees well with those by the MCDRAG,[13] the NSWCAP,[15] and the Beam-Warming scheme.[17] At $M_\infty = 1.2$ and $\beta = 0$ deg, the Beam-Warming scheme overpredicted the pressure drag.

Figure 6 shows the variation of the viscous drag coefficient C_{DV} with Mach number and its comparison for $\beta = 7$ deg. The C_{DV} predicted by the TVD scheme is in close agreement with the MCDRAG and the Beam-Warming predictions in both cases at Mach numbers from 0.91 to 1.2, compared with lower values predicted by the NSWCAP code. It is seen that the viscous drag is gradually decreased with increasing Mach number. A trend similar to Fig. 6 was found for $\beta = 0$ deg. However, the viscous drag in the $\beta = 7$ deg case is about 5–6% smaller than those in the $\beta = 0$ deg case.

Figure 7 shows the comparison of the base drag coefficient C_{DB} for $\beta = 7$ deg. TVD scheme predictions are in reasonable agreement with the MCDRAG code but deviate from Kayser's experiments and the predictions by the Beam-Warming scheme at lower Mach numbers. Note that in Kayser's experi-

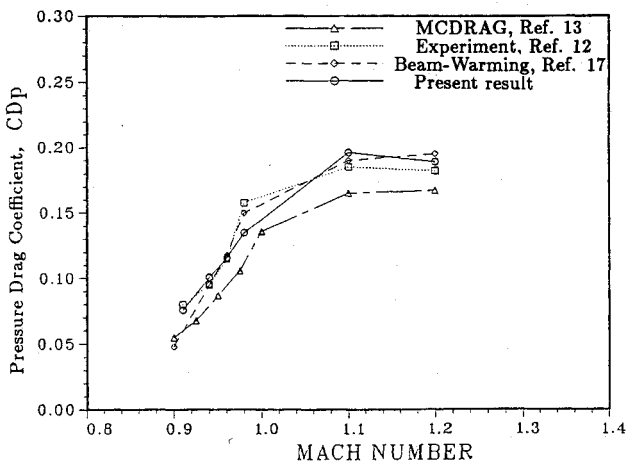

Fig. 5 Variation of pressure drag coefficient with Mach number: $\beta = 7$ deg.

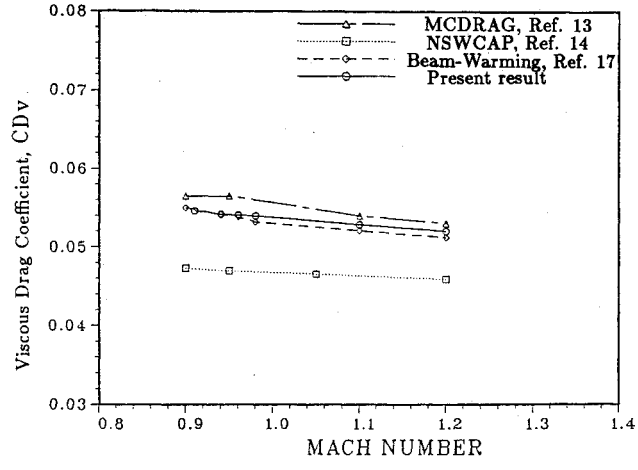

Fig. 6 Variation of viscous drag coefficient with Mach number: $\beta = 7$ deg.

ments a sting is mounted on the projectile base. Hence the sting may cause some disturbances on the base drag. For the case of $\beta = 7$ deg, a substantial decrease in C_{DB}, as shown in Fig. 7, is obtained compared with the case of $\beta = 0$ deg. In the case of $\beta = 0$ deg, the results of the computed base drag at all chosen Mach numbers compared well with the MCDRAG code. Note that negative values of C_{DB} (or net thrust) were found in Kayser's results and in the case of the Beam-Warming scheme at Mach numbers between 0.91 and 0.98; the base drag also decreases with increasing Mach number in that speed range. Hsu et al.[18] commented that the negative base drag obtained by the Beam-Warming scheme is caused by an oscillating pressure distribution along the base.

It should be noted that for the cases of $\beta = 7$ deg at $M_\infty = 0.91$ and 0.96, the present prediction of the pressure coefficient (shown in Fig. 4b) for $R < 0.17$ are positive. However, in Kayser's experiment, the base pressure was measured at only one location at about $R = 0.167$, and a positive pressure coefficient was obtained. The positive pressure coefficient, representing the pressure on the base, results in a negative base drag. If the overall base region, rather than only one location, is taken into account, a nonnegative base drag is obtained. The integration of the pressure along the base produces a correct result. In contrast, the one-point datum produced unreasonable results.

The total drag coefficient C_{D0} obtained from the individual components for $\beta = 7$ deg is presented in Fig. 8. For $0.9 \le M_\infty \le 1.1$, all predicted results indicate that the total

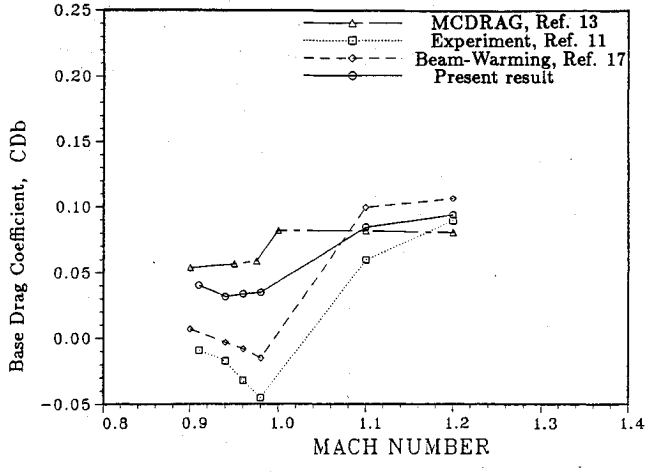

Fig. 7 Variation of base drag coefficient with Mach number: $\beta = 7$ deg.

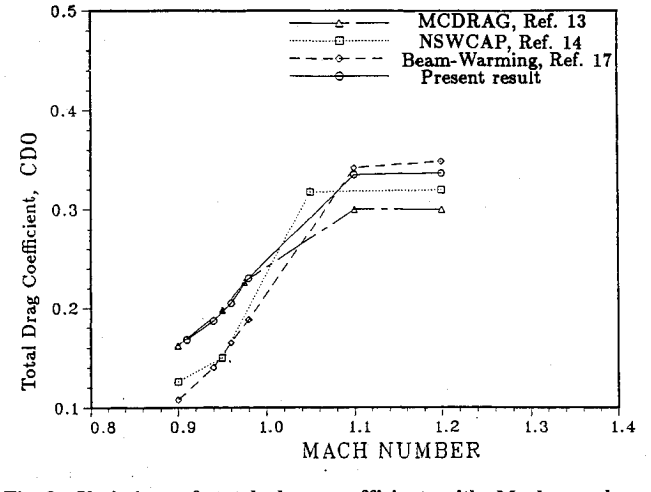

Fig. 8 Variation of total drag coefficient with Mach number: $\beta = 7$ deg.

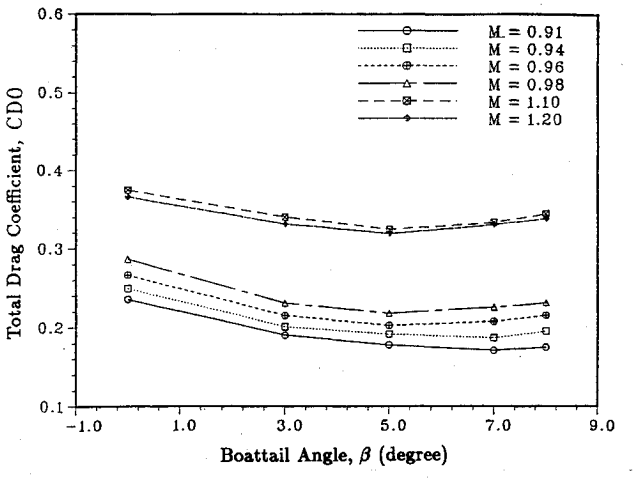

Fig. 9 Variation of total drag coefficient with boattail angle for different Mach numbers.

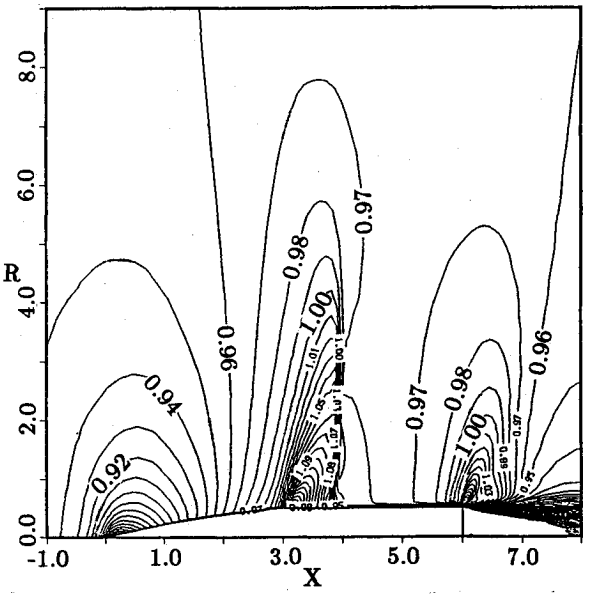

Fig. 10 Mach contour of an SOC projectile with a base bleed: $M_\infty = 0.96$, $I = 0.1$, and $\bar{\omega} = 0.9$.

drag coefficient increases with Mach number. Present predictions of total drag agree well with the MCDRAG code for $M_\infty < 1$ in $\beta = 5$ and 7 deg cases. When $M_\infty > 1$ and $\beta = 7$ deg, differences are noted, which are due to the underprediction of the pressure drag in the MCDRAG code (see Fig. 5); however, the present results are close to the results of the Beam-Warming scheme. For $0.9 < M_\infty < 1.0$, the predicted total drag does not agree well with the result of Beam and Warming as a consequence of the negative base drag provided by the Beam-Warming scheme.

The preceding comparisons provided verification of the present code's accuracy; results will next be presented for optimizing the boattail angle. It was found that the boattail drag coefficient and its change rate at Mach numbers between 0.91 and 0.98 increase with the boattail angle. Moreover, for larger boattail angles ($\beta > 5$ deg), the increasing rate in C_{DBT} was found larger than the decreasing rate in C_{DB}. Figure 9 shows the variation of the total drag coefficient with the boattail angle. Because of the fast increase in the boattail drag for larger boattail angles, an optimal boattail angle for the total drag reduction was found to be at about 5-7 deg for Mach numbers ranging from 0.91 to 1.2.

Although boattailing can substantially reduce the base drag, it induces an additional wave drag on the boattail; however,

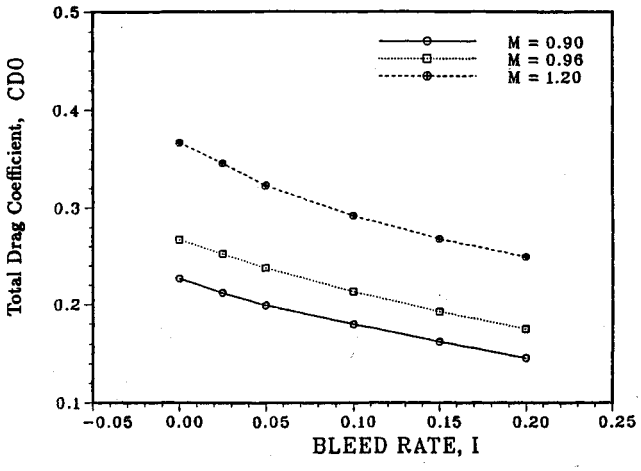

Fig. 11 Variation of total drag coefficient with bleed quantity (rate) for different Mach numbers: $\bar{\omega} = 0.9$.

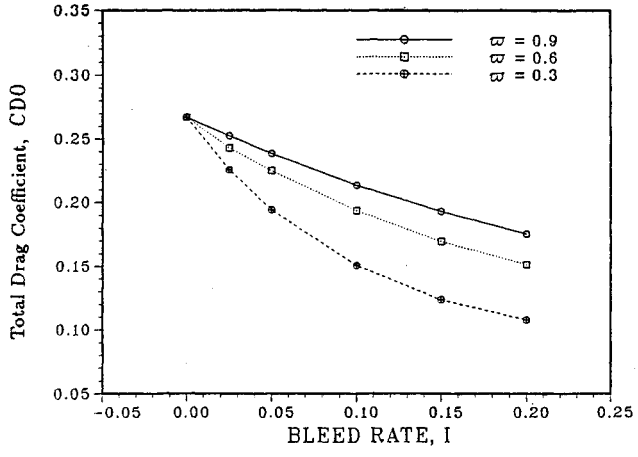

Fig. 12 Variations of total drag coefficient with bleed quantity (rate) for different bleed area ratios: $M_\infty = 0.96$.

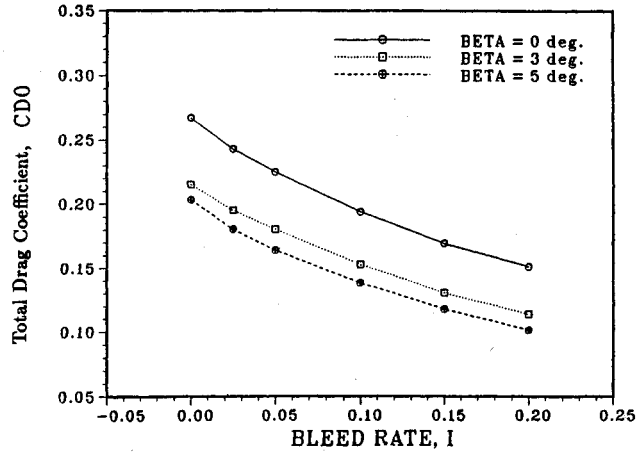

Fig. 13 Variation of total drag coefficient with bleed quantity (rate) for different boattail angles: $M_\infty = 0.96$ and $\bar{\omega} = 0.6$.

the net effect of boattailing is still positive. The reduction in the total drag can be up to 28, 21, and 8% for $\beta = 7$ deg at $M_\infty = 0.91$, 0.96, and 1.2, respectively.

Effect of Base Bleed

The bleed quantity I and the bleed area ratio $\bar{\omega}$ are two parameters in the base bleed method for base drag reduction. The values of these two parameters and the combined effect of base bleed and boattailing were studied.

Five different bleed quantities ($I = 0.025$, 0.05, 0.1, 0.15, and 0.2) and three bleed area ratios ($\bar{\omega} = 0.9$, 0.6, and 0.3) were chosen. Computations were performed on a projectile without boattailing, and the bleed area ratio chosen ranges from 30 to 90% of the base. The bleed region is a circular region that is centered about the symmetric axis, and has an area that is 90% of the base area.

Effect of Bleed Quantity

Figure 10 shows the Mach number contours of an SOC projectile at Mach number of 0.96 with base bleed rate of 0.1. Compared with the results of $I = 0$ (see Fig. 3a) it is found that the supersonic region near the base corner is reduced. The corresponding pressure distribution on the projectile surface was found to be the same as the case of $I = 0$. Namely, the pressure on the projectile surface is independent of the base bleed except at the base where the pressure is increased. Moreover, the peak of the pressure distribution along the symmetry axis, $\xi = \xi_{max}$, is reduced after the base bleed. The computed head drag coefficient C_{DH} and viscous drag coefficient C_{DV} are found to be independent of the base bleed for Mach numbers from 0.9 to 1.2.

The variation of the total drag coefficient with bleed quantity for different Mach numbers is shown in Fig. 11. It can be seen that the total drag decreases with increasing bleed quantity. The total drag reduction is about 36, 34, and 32% for $I = 0.2$ and $M_\infty = 0.9$, 0.96, and 1.2, respectively.

Effect of Bleed Area

The variation of the total drag coefficient for different bleed area ratios at $M_\infty = 0.96$ is shown in Fig. 12. It is seen that the total drag decreases with bleed area ratio and with increasing bleed quantity. For the case of $\bar{\omega} = 0.3$ and $I = 0.2$, the reduction in total drag can be as high as 60% compared with the no base bleed case.

Combined Effect of Base Bleed and Boattailing

In studying the combined effect of base bleed and boattailing on the drag reduction, the projectiles with boattail angles of 3 and 5 deg and bleed area ratio of 0.6 at Mach number of 0.96 are chosen. The bleed quantity ranges from 0.025 to 0.2. It was found that the computed head drag $C_{DH} = 0.03$ is independent of the boattail angle and the bleed quantity; the viscous drags, $C_{DV} = 0.056$ for $\beta = 3$ deg, and $C_{DV} = 0.054$ for $\beta = 5$ deg, are almost unchanged for different bleed quantities. The boattail drag is slightly decreased from 0.0274 to 0.0264 for $\beta = 3$ deg, and from 0.0578 to 0.0469 for $\beta = 5$ deg, as the bleed quantity is increased from 0.025 to 0.2.

Figure 13 shows the variation of the total drag coefficient with bleed quantity for different boattail angles. The total drag is decreased with increasing boattail angle and bleed quantity. A similar result was found for the base drag. Note that for $\beta = 5$ deg, a negative base drag (or thrust) can be obtained for bleed quantity $I > 0.11$. The total drag reduction is as high as 60% for $\beta = 3$ and 5 deg with $\bar{\omega} = 30\%$, and 50% for $\beta = 3$ and 5 deg with $\bar{\omega} = 60\%$, as the bleed quantity is increased from 0 to 0.2. It should be noted that the drag estimate does not take into account the losses due to pumping out the bleed air. If this loss is taken into account, the effectiveness of base bleed on total drag reduction would be decreased.

Conclusion

Transonic flows over a secant-ogive-cylinder-boattail projectile at zero angle of attack have been successfully simulated by solving the axisymmetric thin-layer Navier-Stokes equations, using an implicit, symmetric TVD scheme. To reduce the total drag of a projectile, two methods, boattailing and base bleed, are applied. The effectiveness of each method and the combination of both methods is studied by varying the

values of parameters such as boattail angle in boattailing and bleed quantity and bleed area in base bleed. The computed distributions of surface pressure coefficient on the projectile with different boattail angles at Mach numbers between 0.91 and 1.20 are found to be in close agreement with experimental data. All computed drag components and the total drag of the projectile showed reasonable comparisons with experimental data, semiempirical predictions, and existing numerical results. An optimal boattail angle for total drag reduction is found to be at about 5–7 deg for Mach numbers ranging from 0.91 to 1.2. In addition to boattailing, base bleed is also applied for base drag reduction. It was found that the base drag and the total drag are decreased with bleed area and with increasing bleed quantity. For a projectile at $M_\infty = 0.96$ with bleed quantity of 0.2 and bleed area ratio of 0.3, the reduction in total drag can be as high as 60% for no boattailing, and 50% for 3 and 5 deg boattails with the same bleed quantity and bleed area ratio of 0.6.

Acknowledgment

The authors are indebted to T. H. Moulden at the University of Tennessee Space Institute for critique of the manuscript.

References

[1]Sahu, J., Nietubicz, C. J., and Steger, J. L., "Navier-Stokes Computations of Projectile Base Flow with and without Mass Injection," *AIAA Journal,* Vol. 23, No. 9, 1985, pp. 1348–1355.

[2]Sahu, J., Nietubicz, C. J., and Steger, J. L., "Numerical Computation of Base Flow for a Projectile at Transonic Speeds," AIAA Paper 82-1358, Aug. 1982.

[3]Sedney, R., "Review of Base Drag," U.S. Army Ballistic Research Lab., Rept. 1337, Aberdeen Proving Ground, MD, Oct. 1966.

[4]Tanner, M., "Reduction of Base Drag," *Progress in Aerospace Sciences*, Vol. 16, No. 4, 1975, pp. 369–384.

[5]Sykes, D. M., "Cylindrical and Boat-Tailed Afterbodies in Transonic Flow with Gas Ejection," *AIAA Journal,* Vol. 8, No. 3, 1970, pp. 588–590.

[6]Schetz, J. A., Billig, F. S., and Favin, S., "Approximate Analysis of Axisymmetric Supersonic Base Flows with Injection," *AIAA Journal,* Vol. 18, No. 8, 1980, pp. 867–868.

[7]Addy, A. L., "Thrust-Minus-Drag Optimization by Base Bleed and/or Boattailing," *Journal of Spacecraft and Rockets,* Vol. 7, No. 11, 1970, pp. 1360, 1361.

[8]Bowman, J. E., and Clayden, W. A., "Boat-Tailed Afterbodies at $M = 2$ with Gas Ejection," *AIAA Journal,* Vol. 6, No. 10, 1968, pp. 2029, 2030.

[9]Sullins, G. A., Anderson, J. D., and Drummond, J. P., "Numerical Investigation of Supersonic Base Flow with Parallel Injection," AIAA Paper 82-1001, June 1982.

[10]Deiwert, G. S., "Supersonic Axisymmetric Flow over Boattails Containing a Centered Propulsive Jet," *AIAA Journal,* Vol. 22, No. 10, 1984, pp. 1358–1365.

[11]Kayser, L. D., and Whiton, F., "Surface Pressure Measurements on a Boattailed Projectile Shape at Transonic Speeds," U.S. Army Ballistic Research Lab., ARBRL-MR-03161, Aberdeen Proving Ground, MD, March 1982.

[12]Kayser, L. D., "Base Pressure Measurements on a Projectile Shape at Mach Numbers from 0.91 to 1.20," U.S. Army Ballistic Research Laboratory, ARBRL-MR-03353, Aberdeen Proving Ground, MD, April 1984.

[13]McCoy, R. L., "MCDRAG—A Computer Program for Estimating the Drag Coefficients of Projectiles," U.S. Army Ballistic Research Lab., ARBRL-TR-02293, Aberdeen Proving Ground, MD, Feb. 1981.

[14]Moore, F. G., and Swanson, R. C., "Aerodynamics of Tactical Weapons to Mach Number 3 and Angle of Attack 15°, Part I—Theory and Application," Naval Surface Weapons Center, Dahlgren Lab., NSWC/DL TR-3584, Dahlgren, VA, Feb. 1977.

[15]Moore, F. G., and Swanson, R. C., "Aerodynamics of Tactical Weapons to Mach Number 3 and Angle of Attack 15°, Part II—Computer Program and Usage," Naval Surface Weapons Center, Dahlgren Lab., NSWC/DL TR-3600, Dahlgren, VA, March 1977.

[16]Sahu, J., and Nietubicz, C. J., "Numerical Computation of Base Flow for a Projectile at Transonic Speeds," AIAA Paper 82-1358, Aug. 1982.

[17]Sahu, J., "Drag Predictions for Projectiles at Transonic and Supersonic Speeds," U.S. Army Ballistic Research Lab., Memorandum Rept. BRL-MR-3523, Aberdeen Proving Ground, MD, June 1986.

[18]Hsu, C. C., Shiau, N. H., and Reed, C. W., "Numerical Simulation of Transonic Turbulent Flow Past a Real Projectile," AIAA Paper 88-0218, Jan. 1988.

[19]Shiau, N. H., and Hsu, C. C., "A Diagonalized TVD Scheme for Turbulent Transonic Projectile Aerodynamics Computation," AIAA Paper 88-0217, Jan. 1988.

[20]Yee, H. C., "On Symmetric and Upwind TVD Schemes," *Proceedings of the 6th GAMM Conference on Numerical Methods in Fluid Mechanics*, Gottingen, Germany, Sept. 1985, pp. 399–407.

[21]Baldwin, B. S., and Lomax, H., "Thin-Layer Approximation and Algebraic Model for Separated Turbulent Flows," AIAA Paper 78-257, Jan. 1978.

[22]Nietubicz, C. J., Pulliam, T. H., and Steger, J. L., "Numerical Solution of the Azimuthal-Invariant Thin-Layer Navier-Stokes Equations," AIAA Paper 79-0010, Jan. 1979.

[23]Degani, D., and Schiff, L. B., "Computation of Turbulent Supersonic Flows Around Pointed Bodies Having Crossflow Separation," *Journal of Computational Physics,* Vol. 66, Sept. 1986, pp. 173–196.

[24]Steger, J. L., Nietubicz, C. J., and Heavey, K. R., "A General Curvilinear Grid Generation Program for Projectile Configurations," U.S. Army Ballistic Research Lab., Memorandum Rept. ARBRL-MR-03142, Aberdeen Proving Ground, MD, Oct. 1981.

[25]Sorenson, R. L., "A Computer Program to Generate Two-Dimensional Grids About Airfoils and Other Shapes by the Use of Poisson's Equation," NASA TM-81198, May 1980.

[26]Thompson, J. F., "A General Three-Dimensional Elliptic Grid Generation System on a Composite Block Structure," *Computer Methods in Applied Mechanics and Engineering*, Vol. 64, Nos. 1–3, 1987, pp. 377–411.

[27]Beam, R. M., and Warming, R. F., "An Implicit Factored Scheme for the Compressible Navier-Stokes Equations," *AIAA Journal,* Vol. 16, No. 4, 1978, pp. 393–402.

[28]Pulliam, T. H., and Chaussee, D. S., "A Diagonal Form of an Implicit Approximate Factorization Algorithm," *Journal of Computational Physics,* Vol. 39, No. 2, 1981, pp. 347–363.

[29]Pulliam, T. H., "Euler and Thin-Layer Navier-Stokes Codes: ARC2D, ARC3D," Notes for CFD User's Workshop, Tullahoma, TN, March, 1984.

[30]Pulliam, T. H., and Steger, J. L., "Recent Improvements in Efficiency, and Convergence for Implicit Approximate Factorization Algorithms," AIAA Paper 85-0360, Jan. 1985.

[31]Roe, P. L., "Approximate Riemann Solver, Parameter Vectors, and Difference Schemes," *Journal of Computational Physics,* Vol. 43, No. 2, 1981, pp. 357–372.

[32]Hu, C. L., and Liang, S. M., "Numerical Investigation of Thrust-Reversing Nozzle Using an Implicit TVD Scheme," AIAA Paper 89-2899, July 1989.

[33]Yee, H. C., and Harten, A., "Implicit TVD Schemes for Hyperbolic Conservation Laws in Curvilinear Coordinates," *AIAA Journal,* Vol. 25, No. 2, 1987, pp. 266–274.

[34]Anderson, W. K., Thomas, J. L., and van Leer, B., "A Comparison of Finite Volume Flux Vector Splittings for the Euler Equations," AIAA Paper 85-0122, Jan. 1985.

[35]Fu, J. K., "A Numerical Study on Drag Reduction of Turbulent Transonic Flow over a Projectile," Ph.D. Dissertation, Inst. of Aeronautics and Astronautics, National Cheng Kung Univ., Tainan, Taiwan, ROC, 1991.

Gerald T. Chrusciel
Associate Editor